JOURNAL OF AIRCRAFT
Vol. 41, No. 1, January–February 2004

Effect of Intercycle Ice Accretions on Airfoil Performance

Andy P. Broeren* and Michael B. Bragg†
University of Illinois at Urbana–Champaign, Urbana, Illinois 61801
and
Harold E. Addy Jr.‡
NASA John H. Glenn Research Center at Lewis Field, Cleveland, Ohio 44135

Results are presented of an experimental study designed to characterize and evaluate the aerodynamic performance penalties of residual and intercycle ice accretions that result from the cyclic operation of a typical aircraft deicing system. Icing wind-tunnel tests were carried out on a 36-in. chord NACA 23012 airfoil section equipped with a pneumatic deicer for several different Federal Air Regulation 25 Appendix C cloud conditions. Results from the icing tests showed that the intercycle ice accretions were much more severe in terms of size and shape than the residual ice accretions. Molds of selected intercycle ice shapes were made and converted to castings that were attached to the leading edge of a 36-in. chord NACA 23012 airfoil model for aerodynamic testing. The aerodynamic testing revealed that the intercycle ice shapes caused a significant performance degradation. Maximum lift coefficients were typically reduced about 60% from 1.8 (clean) to 0.7 (iced) and stall angles were reduced from 17 deg (clean) to 9 deg (iced). Changes in the Reynolds number (from 2.0×10^6 to 10.5×10^6) and Mach number (from 0.10 to 0.28) did not significantly affect the iced-airfoil performance.

Nomenclature

C_d	=	drag coefficient
C_l	=	lift coefficient
$C_{l,\max}$	=	maximum lift coefficient, coincident with α_{stall}
$C_{l,\alpha}$	=	lift-curve slope
C_m	=	quarter-chord pitching-moment coefficient
c	=	airfoil chord length
k	=	ice-roughness height or thickness
M	=	freestream Mach number
Re	=	Reynolds number based on chord
x	=	chordwise position along airfoil
y	=	normal position from airfoil chord line
α	=	airfoil angle of attack
α_{stall}	=	stalling angle of attack, coincident with $C_{l,\max}$

Introduction

THE cyclic operation of typical pneumatic aircraft deicing systems leads to the formation of residual and intercycle ice accretions. For example, pneumatic boots operated in automatic mode are usually inflated and deflated at either 1 or 3-min intervals, depending upon the severity of icing. The ice accretion present on the deicer surface just before its initial activation is the preactivation ice. After the system has been cycled a sufficient number of times, the periodic activation and ice accretion cycle reaches steady state. After steady state has been reached, intercycle ice refers to the ice shape as it exists immediately before subsequent activations of the deicer. This is not to be confused with residual ice, which refers to any ice that remains on the surface immediately after the deicer activation. This paper addresses the characteristics of residual and intercycle ice accretions for a given airfoil and deicing system along with the aerodynamic performance penalties of intercycle ice accretions.

The characteristics of residual and intercycle ice accretions have been the subject of several previous investigations. Shin and Bond[1] analyzed the ice accretions for several different deicing systems installed on an NACA 0012 airfoil. The reported results were for 1-min cycling times and showed that the deicers generally cleaned the leading edge, leaving little residual ice. The intercycle ice, therefore, would accrete in the 1-min period leading up to the deicer operation. The height of the intercycle ice roughness, normalized by chord, varied from approximately $k/c = 0.002$–0.010, depending on the icing condition, that is, glaze or rime, and the type of deicer. Shin and Bond[1] concluded that the intercycle ice would have an effect on airfoil and wing performance and that uniformly distributed roughness may not be an appropriate simulation of the actual intercycle ice. No aerodynamic measurements were performed during the study.

Aerodynamic performance effects of residual and intercycle ice were included in some of the previous research. Albright et al.[2] measured the drag coefficient before and after the operation of a pneumatic deicer on a NACA 65_1-215 airfoil. The general results showed that the intercycle ice (before deicer operation) caused a higher drag coefficient than the residual ice (after deicer operation), both of which were higher than for the clean airfoil. Similar research was carried out by Bowden[3] for an NACA 0011 airfoil. Bowden also showed how the lift coefficient decreased as ice was accreted and then increased when the boot was cycled and the ice shed. The results of these studies were taken from a recent review of residual ice characteristics and performance penalties, and the reader is encouraged to consult Reichhold and Bragg[4] for more details. Although these reports provided meaningful data on the performance effects of residual and intercycle ice accretions, a major shortcoming was that the data were acquired at fixed angle of attack. Therefore, the change in the airfoil stall characteristics was not documented.

The effect of intercycle ice accretions on performance of an natural laminar flow (NLF)-0414 airfoil was considered by Gile-Laflin and Papadakis[5] and by Jackson and Bragg.[6] Intercycle ice shapes were documented for tests on a 48-in. chord NLF-0414 airfoil model for one icing cloud condition and for 1-min cycling times. Results from four different deicing systems were obtained. Gile-Laflin and Papadakis[5] conducted aerodynamic testing on a 48-in. chord NLF-0414 airfoil model using ice-shape castings produced from molds taken during the icing tests. Jackson and Bragg[6] conducted aerodynamic testing on an 18-in. chord NLF-0414 airfoil model using

Received 3 April 2003; revision received 9 June 2003; accepted for publication 11 June 2003.

*Research Scientist, Department of Aeronautical and Astronautical Engineering, 306 Talbot Laboratory, 104 South Wright Street; broeren@uiuc.edu. Member AIAA.

†Professor and Head, Department of Aeronautical and Astronautical Engineering, 306 Talbot Laboratory,104 South Wright Street; mbragg@uiuc.edu. Associate Fellow AIAA.

‡Research Engineer, Icing Branch, Mail Stop 11-2, 21000 Brookpark Road; Gene.Addy@nasa.gov. Member AIAA.

two-dimensional, that is, no spanwise variation in cross section, ice-shape simulations that were geometrically scaled from ice tracings. The degradation in maximum lift was on the order of 30%, and results from both aerodynamic tests agreed fairly well. However, the effect of different cloud conditions and cycling times was not addressed.

The brief literature survey shows that there are valuable studies in the public domain, but more information is needed. Particularly, the effect of actual residual and intercycle ice accretions formed at one angle of attack on airfoil performance over its larger operating range is largely unknown. Recently, some questions have been raised concerning the effects of residual and intercycle ice for turbopropeller and piston aircraft employing pneumatic boot deicing systems.[7,8] Because little relevant data were available, the Federal Aviation Administration (FAA) in collaboration with NASA commissioned a study to assess the potential aerodynamic severity of residual and intercycle ice accretions. This effort involved researchers at the University of Illinois and B. F. Goodrich Aerospace Deicing and Specialty Systems Division, with participation by some aircraft manufacturers. More details on the scope of this work are given by Riley et al.[9]

The objectives of this study were to characterize the nature of residual and intercycle ice accretions, measure the resulting aerodynamic performance penalties of selected intercycle ice accretions and determine if more detailed study was warranted. A NACA 23012 airfoil was selected for this study because it is representative of wing airfoil sections used on some aircraft currently in operation. The airfoil was equipped with a pneumatic deicing boot provided by B. F. Goodrich. The intercycle ice accretions were generated in the B. F. Goodrich icing wind tunnel and were molded using procedures developed at NASA John H. Glenn Research Center. From these molds, castings were made that were attached to the leading edge of a NACA 23012 airfoil in the NASA Langley Research Center Low-Turbulence Pressure Tunnel (LTPT). Subsequent airfoil performance measurements were made over a large range of angles of attack and Reynolds and Mach numbers.

Experimental Facilities and Apparatus

Icing Tests

The ice-accretion testing was conducted at the B. F. Goodrich Icing Wind Tunnel (IWT). The IWT is a closed-loop, refrigerated wind tunnel with a test section 22 in. wide by 44 in. high by 60 in. long. The icing cloud in the tunnel is generated by NASA-type, atomizing nozzles mounted in seven spray bars located in the settling chamber upstream of the test section. The icing conditions selected for this experiment were based on Federal Air Regulation FAR 25 Appendix C and covered a range of conditions including rime, mixed, and glaze icing for both continuous maximum (CM) and intermittent maximum (IM) cases. For most of the test runs, the airspeed was set at the tunnel maximum of 200 mph. This corresponded to a Reynolds number of 6.5×10^6 and a Mach number of 0.27 (at 14°F). Two angles of attack were selected for the tests, 0 and 4 deg.

The NACA 23012 airfoil model used for the icing tests had a 36-in. chord by 22-in. span and was mounted horizontally in the IWT. It was machined from aluminum and was designed with a removable leading edge as shown in Fig. 1. The removable leading-edge design facilitated the ice molding process. The ice molds were subsequently used to make castings for the aerodynamic testing. The model leading edge was recessed to accommodate a flush-mounted B. F. Goodrich-type 29S pneumatic deicer. The deicing boot had five spanwise tubes, two of which were 1.25 in. wide and three that were 1 in. wide (cf. Fig. 1). The deicing system was sized and designed for the 36-in. chord NACA 23012 airfoil at turboprop aircraft speeds. When installed on the model in the tunnel, the deicer was connected to a larger pneumatic deicer outside the tunnel to obtain the proper inflation rate. The deicer operation was computer controlled and was set up for either 1- or 3-min cycles. The two deicer cycle times, 1- and 3-min, were used primarily for the IM and CM icing conditions, respectively.

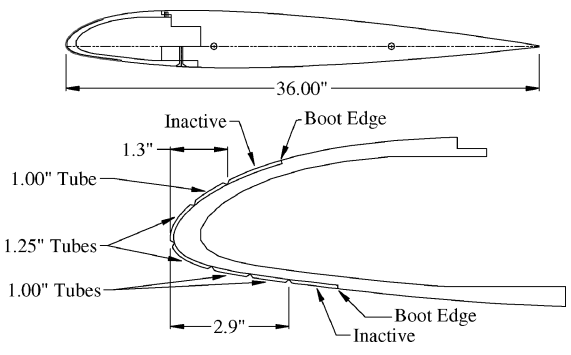

Fig. 1 Cross-sectional schematic drawing of the NACA 23012 icing wind-tunnel model with removable leading edge and deicer.

Table 1 Test conditions for the intercycle ice accretions used for aerodynamic testing

Ice shape	Angle of attack, deg	Static temperature, °F	Droplet MVD,[a] μm	Cloud LWC,[b] g/m^3	Spray time, min	Boot cycle, min
290	0	14	20	0.45	12	3
296	0	21	20	0.65	12	3
312	0	21	40	0.25	12	3
332	0	−4	40	0.40	3	1

[a]Median volumetric diameter (MVD). [b]Liquid water content (LWC).

Total run time was determined to be that which had allowed the deicer to reach a steady state in terms of amount of ice removed per cycle. In general, the ice accretions reached a steady state after two or three deicer cycles. Three deicer cycles were used for the IM cases, so that the run time was 3 min, not including time to activation. Four deicer cycles were used for the CM cases, so that the run time was 12 min, not including time to activation.

A primary objective of the icing tests was to obtain high-fidelity representations of the ice accretions for use in aerodynamic performance tests. The results of the ice-accretion testing showed that the pneumatic deicer generally cleaned the leading edge well, leaving little residual ice. However, the intercycle accretions tended to have more ice on the leading edge and, in some cases, protuberances on the upper surface. These intercycle shapes were expected to cause greater performance degradation and, therefore, were selected for aerodynamic testing. The four ice shapes selected for aerodynamic testing were from runs 290, 296, 312, and 322. The test conditions for these shapes are summarized in Table 1. Ice tracings and photographs are given for these ice accretions in Figs. 2–5. Molds[10] were made for each of these ice accretions. The castings produced from these molds preserved virtually all of the ice accretions features shown in Figs. 2–5. These four ice shapes provided a reasonable variation in cloud conditions and ice-shape type. For example, ice shape 290 (cf. Fig. 2) represents a mixed glaze–rime shape for a CM case. Ice shapes 296 and 312 (cf. Figs. 3 and 4) are both glaze-type shapes, but the ridgelike features on the upper surface are quite different. This was most likely caused by the difference in droplet "median volumetric diameter" (MVD), which was 20 μm for ice shape 296 and 40 μm for ice shape 312. Finally, ice shape 322 (cf. Fig. 5) represents both rime ice and IM cases. The icing tests yielded several other important results pertaining to the operation of pneumatic deicers and the resulting ice accretions. Broeren and Bragg[11] and Broeren et al.[12] present a more detailed treatment of the icing test results along with the experimental methods.

Aerodynamic Tests

All aerodynamic testing was carried out at NASA Langley Research Center, using the LTPT. The LTPT is a closed-return wind tunnel that is principally used for two-dimensional airfoil testing and is described in detail in Refs. 13 and 14. It can be operated at stagnation pressures from near vacuum to 147 psia (except 15–20 psia) and over a Mach number range of 0.05–0.40. A heat exchanger and nine turbulence reduction screens are located in the inlet settling chamber. The contraction ratio is 17.6:1, and the test section

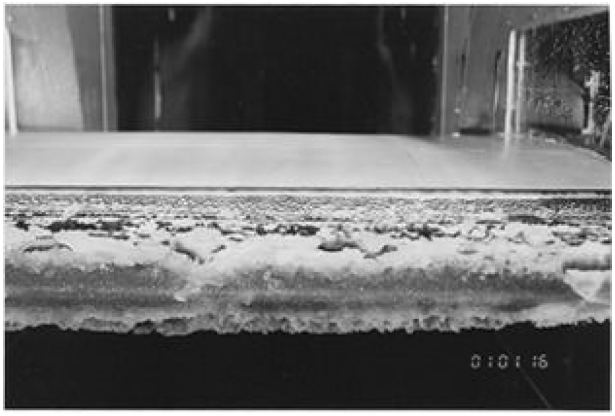

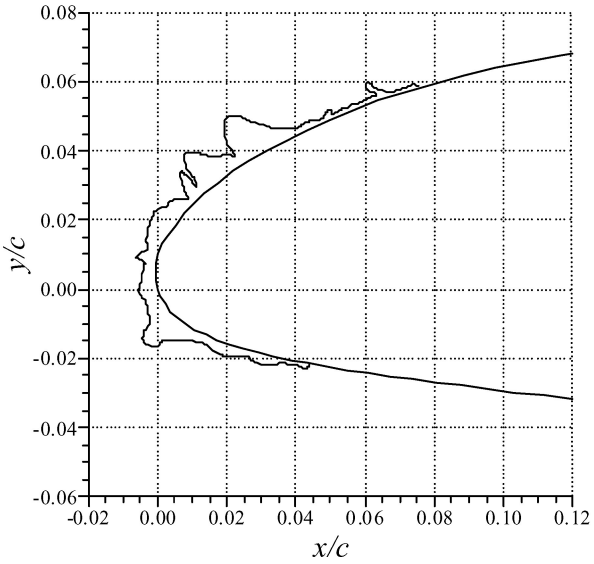

Fig. 2 Photograph and tracing of ice shape 290 (cf. Table 1).

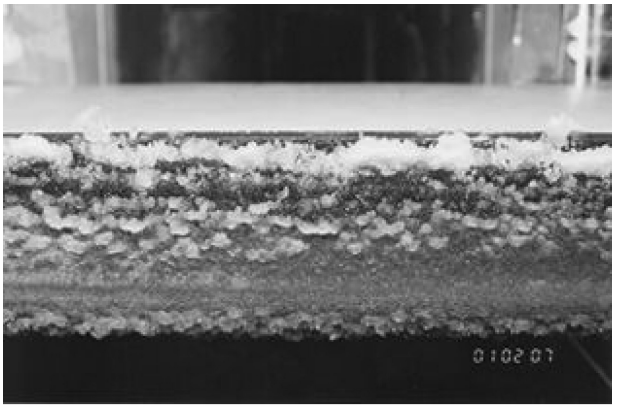

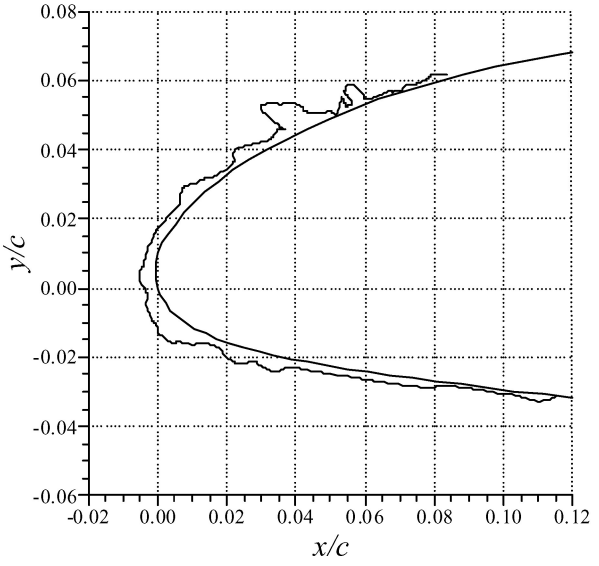

Fig. 3 Photograph and tracing of ice shape 296 (cf. Table 1).

dimensions are 36 in. wide by 90 in. high by 90 in. long. The tunnel was designed for two-dimensional airfoil testing with model chord lengths up to 36-in. (Ref. 13). The freestream turbulence intensity levels were about 0.1% or less for the operating conditions used in this investigation.[14]

The 36-in. chord NACA 23012 airfoil model was supported horizontally across the width of the test section between two 34.5-in.-diam circular endplates. The endplates were flush with the sidewalls and rotated for angle-of-attack adjustment. They also contained a section of porous plate for sidewall boundary-layer control. This sidewall venting system was originally developed for testing high-lift airfoil configurations, and a detailed description is given by Paschal et al.[15] During this study, some runs were performed with and without sidewall venting, and there was very little difference in the results. All of the data presented here were acquired with sidewall venting, except at $Re = 2.0 \times 10^6$ because sidewall venting was not available for this condition.

The NACA 23012 airfoil model was machined aluminum and had recessed openings for pressure instrumentation. The model was designed and built with a removable leading edge. There was a single baseline, or clean leading edge and an alternate leading edge. The ice-shape castings were mounted to the alternate leading edge. This method simulated the actual ice accretion with very high fidelity. In addition, an instrumentation slice was installed near the model midspan. The instrumentation slice was cut out of stainless steel to match the ice-shape cross section and had pressure taps distributed around the ice-shape contour. This allowed for measurements that provided a reasonable representation of the pressure distribution around the ice shape and also provided pressures for determination of the lift and pitching moment coefficients. The baseline model had 67 static pressure orifices along the main chordwise row and 17 orifices in a spanwise row located at $x/c = 0.70$ on the upper surface. The photograph in Fig. 6 shows the model mounted in the test section, with ice-shape casting simulation and pressure instrumentation slice attached to the airfoil leading edge.

The LTPT was equipped with a three-component force balance; however, it was designed for operation with high-lift airfoil systems and for higher dynamic pressures than were run in this experiment. Therefore, the data from the force balance were deemed unreliable except at the higher dynamic pressures, and the lift and pitching moment data were generally obtained from the integration of surface static pressures. These data were compared to the force-balance data for large values of dynamic pressure and excellent agreement was observed for both clean and iced configurations. Therefore, no force-balance data are presented here. Drag coefficients were calculated from wake pressures measured with a wake rake using the standard moment-deficit method. For data collection, 1-deg angle-of-attack increments were used, except for the wake drag, which was acquired in 2-deg increments. Corrections to the integrated performance coefficients accounting for solid and wake blockage and streamline curvature were applied to the data during postprocessing using the methods of Allen and Vincenti.[16]

The experimental uncertainty in the performance coefficients was estimated using the methods of Kline and McClintock[17] and Coleman and Steele[18] for 20:1 odds. Table 2 lists these uncertainties for a set of pressure-derived coefficients and the angle of attack. The values listed were from data on the clean airfoil at $Re = 7.5 \times 10^6$ and $M = 0.21$. For lower Reynolds and Mach numbers,

Table 2 Estimated experimental uncertainties

Aerodynamic quantity	Reference value	Absolute uncertainty	Relative uncertainty, %
α	8.00 deg	±0.02 deg	±0.25
C_p	−1.025	±0.040	±3.90
C_l	1.012	±0.009	±0.89
C_m	−0.0101	±0.0019	±18.81
C_d	0.0088	±0.0004	±4.55

Table 3 Aerodynamic performance test matrix

Reynolds number	Mach number			
	0.10	0.12	0.21	0.28
2.0×10^6	Clean, iced		Clean	
3.5×10^6		Clean, iced		
7.5×10^6		Clean, iced	Clean, iced	Clean, iced
10.5×10^6		Clean, iced		Clean, iced

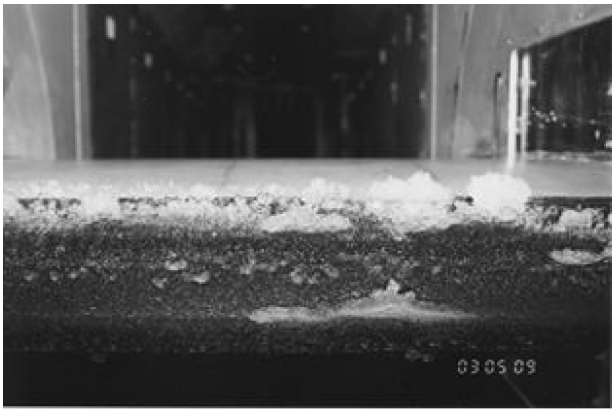

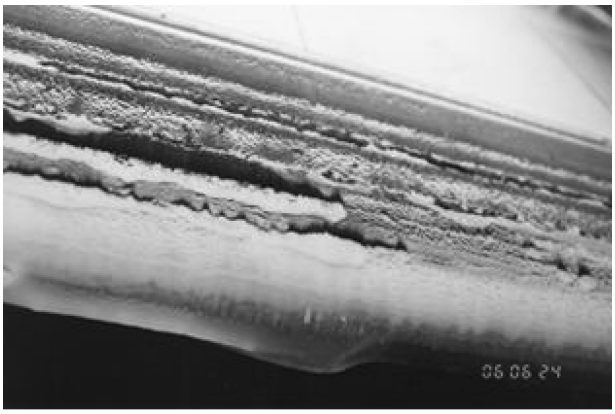

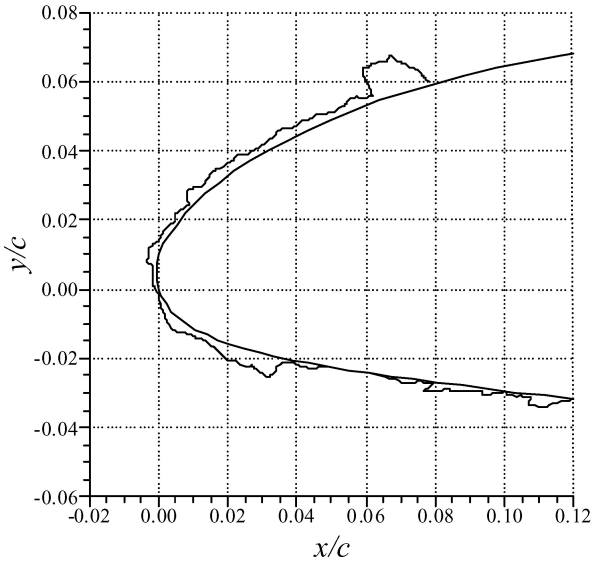

Fig. 4 Photograph and tracing of ice shape 312 (cf. Table 1).

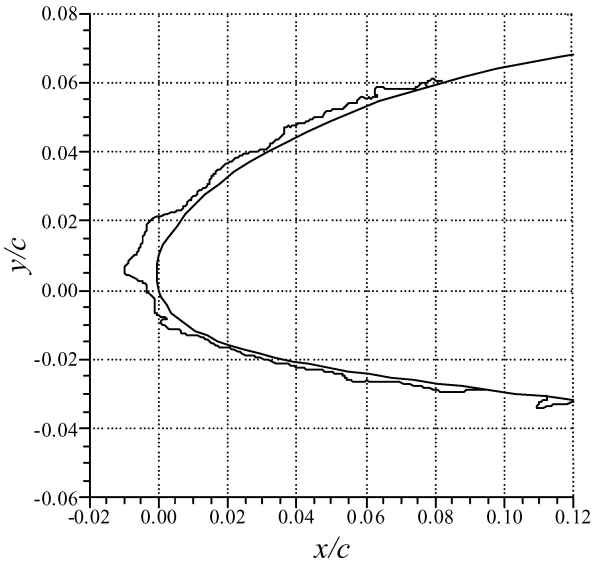

Fig. 5 Photograph and tracing of ice shape 322 (cf. Table 1).

the experimental uncertainties were slightly higher than those shown, whereas higher Reynolds and Mach number conditions had uncertainties that were slightly lower than those shown in Table 2. All of the estimated uncertainties were acceptable for the purposes of this investigation. The relative uncertainty in C_m seems very large for this example because of the small reference value. For cases where the C_m values were larger, for example, in the iced airfoil case, the absolute uncertainty would be similar, therefore, resulting in a lower relative uncertainty. In addition, a repeatability analysis provided by NASA showed that run-to-run variations in the coefficients were much smaller than these uncertainties.

The test matrix was selected to yield a broad range of Reynolds and Mach numbers with the high end being applicable to turbopropeller and piston-engine aircraft as constrained by the limitations of the facility. Table 3 summarizes these conditions for both the clean and iced configurations. In addition to these configurations, standard roughness in the form of 40- and 80-grit sandpaper was also tested. The sandpaper covered the airfoil leading edge from $x/c = 0.07$ on the upper surface to $x/c = 0.10$ on the lower surface.

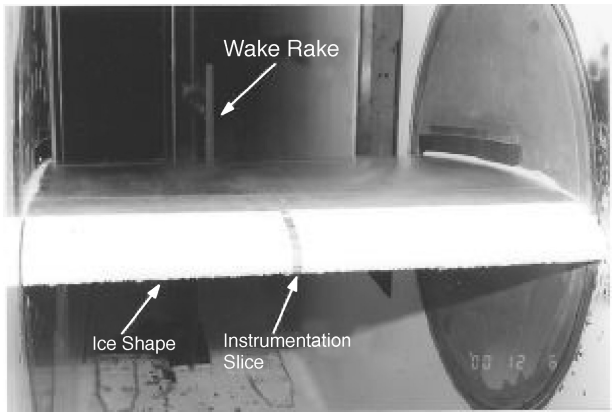

Fig. 6 Photograph of NACA 23012 airfoil model with ice shape in the LTPT test section.

The nominal size of commercial carborundum is approximately 0.0205 in. ($k/c = 0.00057$) and 0.0083 in. ($k/c = 0.00023$) for 40 and 80 grit, respectively.[19] This height did not include the thickness of the paper backing that was approximately one and a half times as large as the roughness itself. Additionally, this was attached to the model surface with 0.003-in.-thick double-sided tape.

Results and Discussion

Clean-Airfoil Aerodynamics

Overall, the clean-airfoil results followed classic airfoil behavior and compared favorably with historical data and computational results. Figure 7 shows the effect of Reynolds number at constant Mach number on the performance coefficients. The maximum lift coefficient increased by approximately 0.10 from $Re = 3.5 \times 10^6$ to $Re = 7.5 \times 10^6$. Conventional results were also observed in the drag data, where the drag coefficients tended to decrease with increasing Reynolds number from $Re = 3.5 \times 10^6$ to $Re = 7.5 \times 10^6$. These trends were also comparable to previous LTPT results for the NACA 0012 airfoil. For example, Ladson[20] analyzed data from performance tests on a NACA 0012 airfoil having a 24-in. chord, acquired with solid sidewalls (no sidewall boundary-layer control) over a large matrix of Reynolds and Mach numbers. Classic airfoil behavior was observed for Mach number variations at constant Reynolds number. The lift-curve slope increased with Mach number, but $C_{l,\max}$ decreased about 0.10 from $M = 0.12$ to 0.28 at $Re = 10.5 \times 10^6$. Typical Mach number effects were observed in the drag and pitching moment data as well.

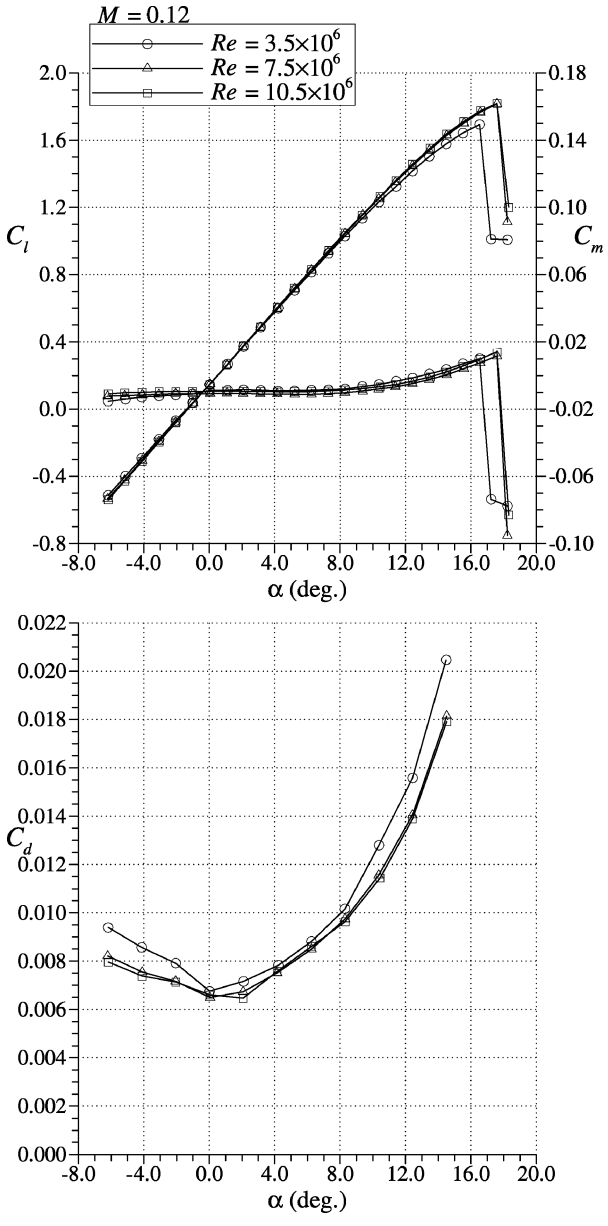

Fig. 7 Effect of Reynolds number at constant Mach number on the performance of the clean NACA 23012 airfoil.

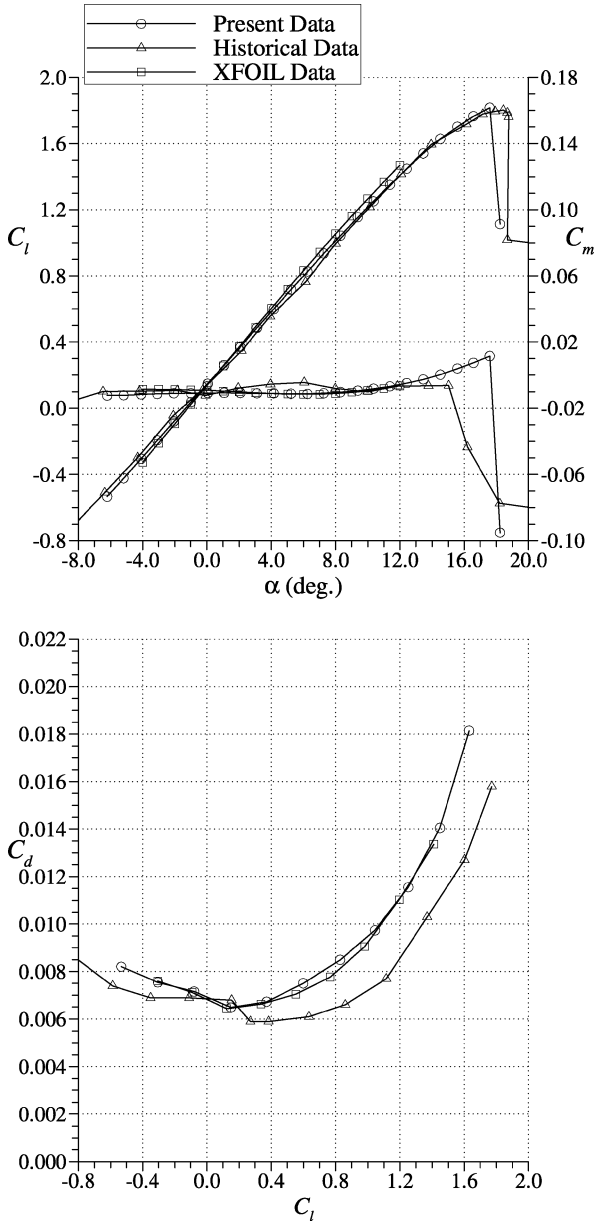

Fig. 8 Comparison of clean NACA 23012 airfoil performance (at $Re = 7.5 \times 10^6$, $M = 0.12$) from the present study with historical data from Abbott and von Doenhoff[21] (at $Re = 8.8 \times 10^6$, $M < 0.17$) and XFOIL data with fixed transition (at $Re = 7.5 \times 10^6$, $M = 0.12$).

The present data were compared to historical data and computational results for further validation as shown in Fig. 8. Figure 8 shows that the present data at $Re = 7.5 \times 10^6$ and $M = 0.12$ compare favorably to data from Abbott and von Doenhoff[21] at $Re = 7.5 \times 10^6$ and $M < 0.17$. (The exact Mach number was not given.) There is excellent agreement in the lift coefficient data, with the $C_{l,\max}$ values being nearly identical. There is also excellent agreement in the pitching moment coefficient in the linear-lift range before stall. The drag coefficients for the historical data were significantly lower than for the present data. This may have been caused by the seams in the airfoil model due to the removable leading-edge design. The removable leading edge joined the main body at $x/c = 0.21$ on the upper and lower surface. Ideally this spanwise-running seam would have been smooth to not cause any flow disturbance. In practice, this was difficult to achieve, and it is possible that there

was enough misalignment to cause boundary-layer transition at this location.

The effect of these seams were investigated using XFOIL,[22] which is an airfoil analysis code that couples a panel method flowfield solver to an integral boundary-layer formulation. This code allowed boundary-layer transition to be fixed at $x/c = 0.21$ for angles of attack where natural transition would occur downstream of this location. As shown in Fig. 8, the XFOIL drag coefficient results compared favorably with the present data. The lift coefficient plot shows that the XFOIL results agreed very well with both sets of experimental data up to about 9-deg angle of attack. At this point and for higher angles, XFOIL overpredicted the lift coefficient. This is a common feature of XFOIL results, in the authors' experience. Although this fixed-transition calculation is by no means conclusive, it does show that the removable leading edge (plus pressure taps, etc.) may have played a role in the departure of drag values from the Abbott and von Doenhoff[21] data. This sort of tradeoff was expected, given the necessary compromises in model quality required to perform the ice-shape testing. Broeren and Bragg[11] and Broeren et al.[12] provide more analysis of the NACA 23012 airfoil data.

Iced-Airfoil Aerodynamics

The performance penalties due to the intercycle ice shapes were found to be very severe. This is shown in Fig. 9 for $Re = 7.5 \times 10^6$ and $M = 0.21$. Three of the four ice-shape castings mounted to the airfoil leading edge (290, 296, and 312) caused nearly the same performance degradation, despite their differences in geometry. The maximum lift coefficient for these shapes was in the range of 0.65–0.75. This represents approximately a 60% reduction from the clean value of 1.8. The stalling angle was reduced from 17.5 to about 8.5 deg. Furthermore, significant degradations in the iced-airfoil lift coefficients was apparent for angles of attack greater than 4 deg. Ice shape 322 was formed from 1-min boot cycles in rime-ice conditions, and it resulted in a slightly lower maximum lift penalty of about 50%. All of the ice-shape castings caused a significant change in the airfoil pitching moment. In the clean case, the pitching moment was nearly constant over the linear-lift range. With the ice shapes attached to the airfoil, the pitching moment had a strong angle-of-attack dependence. The drag data showed at least a three-fold increase in the minimum C_d for three of the four shapes. The ice-shape 322 case had a smaller increase in drag, probably because the shape was smaller and smoother.

The NACA 23012 airfoil section was also tested with 40- and 80-grit sandpaper applied to the leading edge. This test was performed to compare the performance degradation due to a standard, or uniformly distributed, roughness to the performance degradation due to the ice-accretion castings. The use of sandpaper as standard roughness is advantageous because it is easily duplicated for testing in other facilities or in-flight. Figure 10 shows that the sandpaper

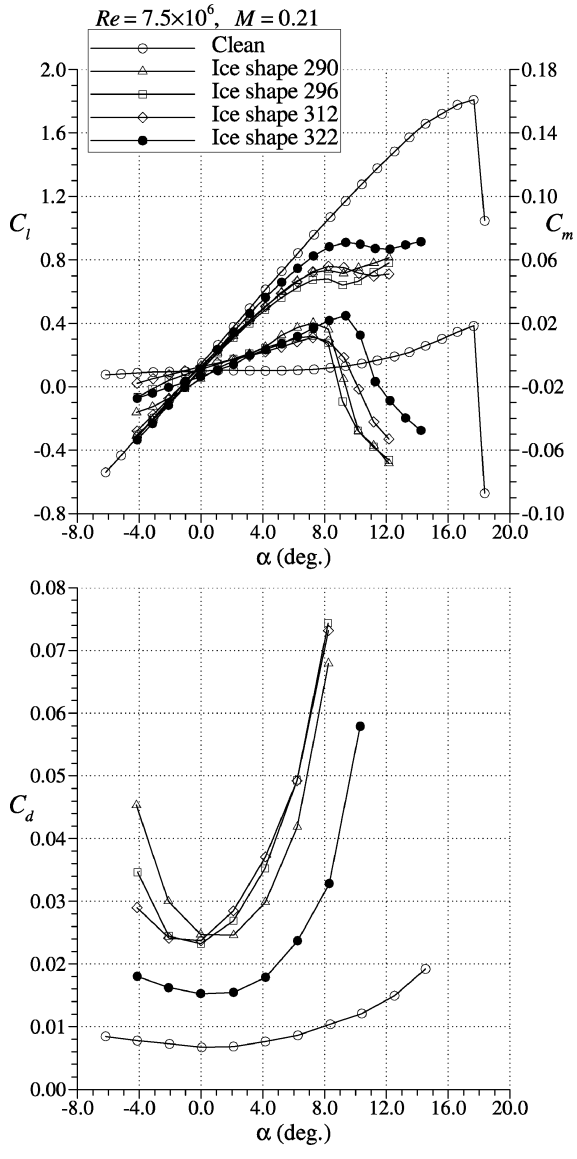

Fig. 9 Effect of intercycle ice accretion simulations on the performance of the NACA 23012 airfoil.

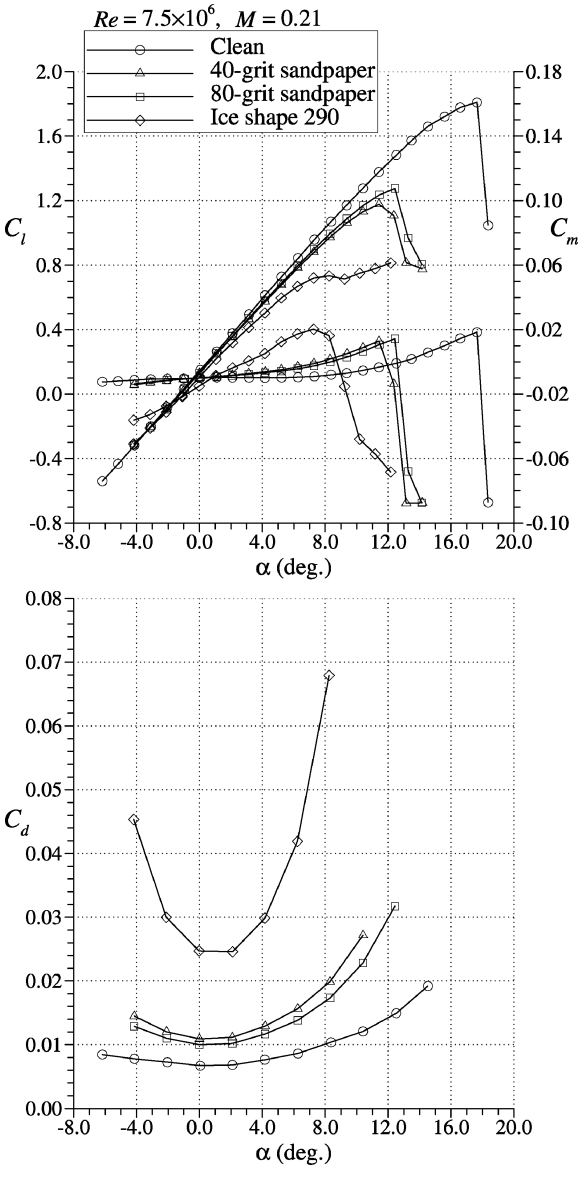

Fig. 10 Effect of 40- and 80-grit sandpaper on the performance of the NACA 23012 airfoil.

performance penalties were about half that of the ice-shape castings. The average reduction in $C_{l,\max}$ was about 33% with α_{stall} being reduced from 17.5 down to about 12 deg. The drag values for the airfoil with sandpaper were generally closer to the clean case than with the ice-shape castings attached. The chief short coming of the sandpaper simulation was that the roughness heights were not close to those of the actual ice accretions. For example, the nominal height (ignoring the larger ridgelike features) of ice shape 290 was $k/c = 0.0056$, whereas the 40-grit sandpaper roughness height was nearly 10 times smaller at $k/c = 0.00057$. Furthermore, the sandpaper simulation did not capture any of the ridgelike features of the intercycle ice accretions.

Reynolds and Mach Number Effects

The effect of Reynolds and Mach number variation was investigated for all of the ice shapes. An example of these effects is shown in Figs. 11 and 12 for the airfoil with the ice-shape 290 casting attached. The lift coefficient data in Fig. 11 show that there was a small increase in $C_{l,\alpha}$ and $C_{l,\max}$ from $Re = 2.0 \times 10^6$ to 3.5×10^6, but there was virtually no change for the higher Reynolds numbers. The drag data exhibited a similar trend where the largest variation occurred from $Re = 2.0 \times 10^6$ to 3.5×10^6. Figure 12 shows that

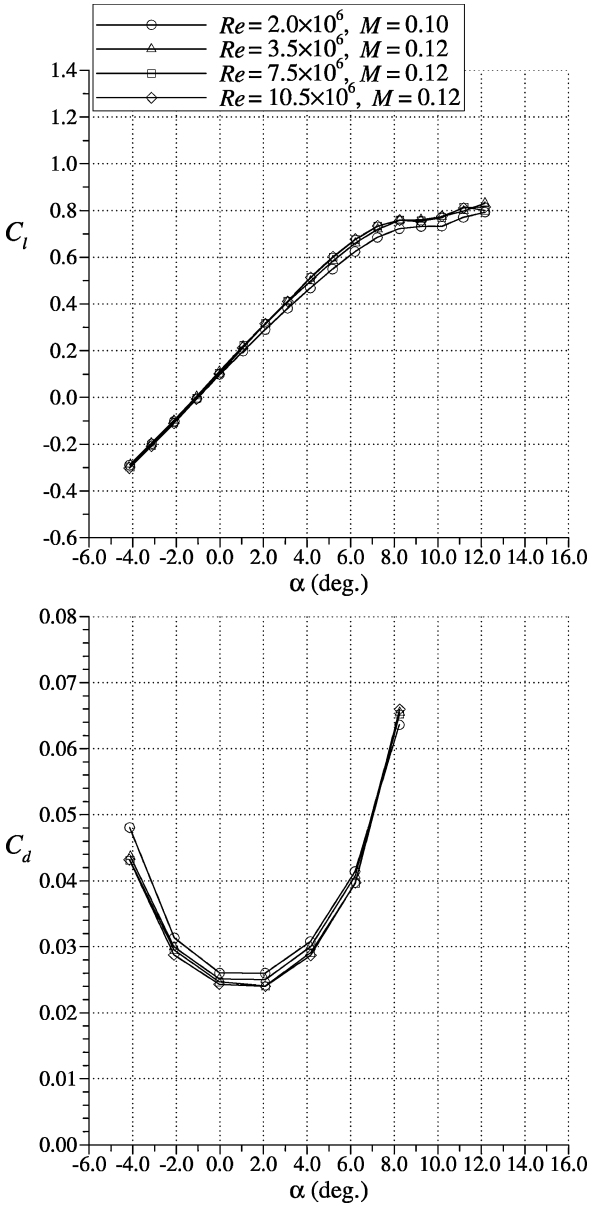

Fig. 11 Effect of Reynolds number on the performance of the NACA 23012 airfoil with ice shape 290.

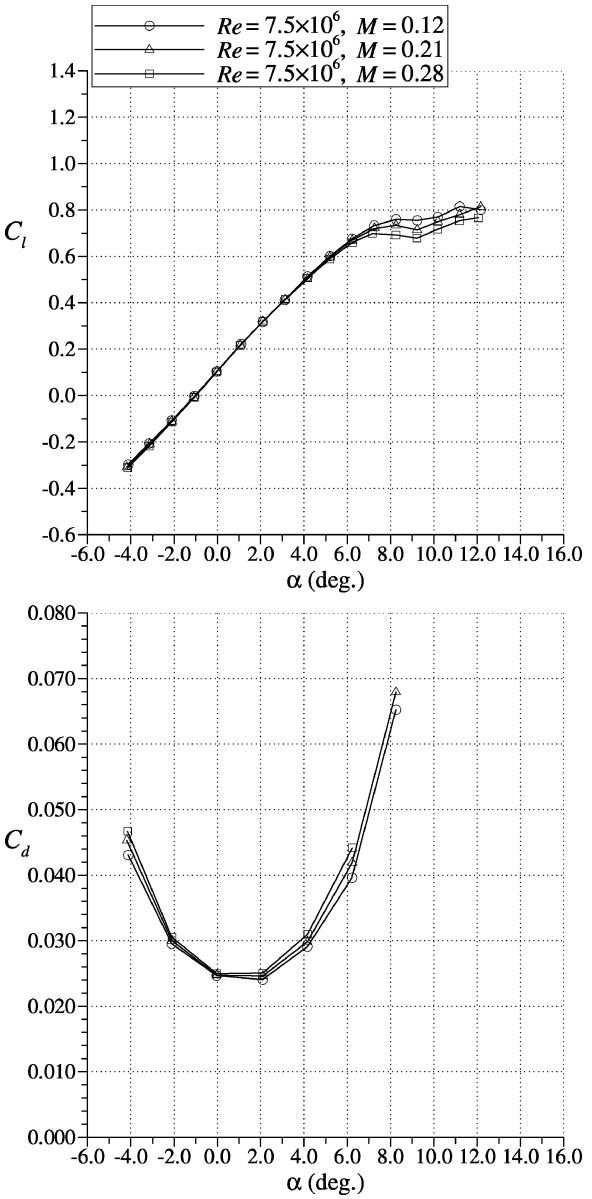

Fig. 12 Effect of Mach number on the performance of the NACA 23012 airfoil with ice shape 290.

there was a measurable variation in $C_{l,\max}$ with Mach number at constant Reynolds number. The drag coefficients tended to increase slightly with increasing Mach number at higher and lower angles of attack. These trends were similar to the clean case, where $C_{l,\max}$ decreased with increasing Mach number and the drag increased. However, these differences were very small relative to the overall performance degradation due to the ice shape.

These Reynolds and Mach number trends were generally observed for all of the iced-airfoil configurations tested. The effect of Reynolds number on the maximum lift coefficient is summarized in Fig. 13. As already indicated, there is only a minor increase (less than 0.05 in C_l) in maximum lift coefficient from $Re = 2.0 \times 10^6$ to 10.5×10^6, for the ice-shape castings. This increase was more significant (approximately 0.10 in C_l) with sandpaper over the leading edge. Figure 14 illustrates that the slight decrease in $C_{l,\max}$ over the Mach number range tested was similar for all of the ice-shape castings. The Mach number behavior was different in the case of the sandpaper as the opposite trend is shown for the 80-grit case. Both Figs. 13 and 14 show the difference in $C_{l,\max}$ performance with sandpaper over the leading edge vs the intercycle ice shapes.

The Reynolds and Mach number trends observed for the iced-airfoil cases are consistent with previous research performed by

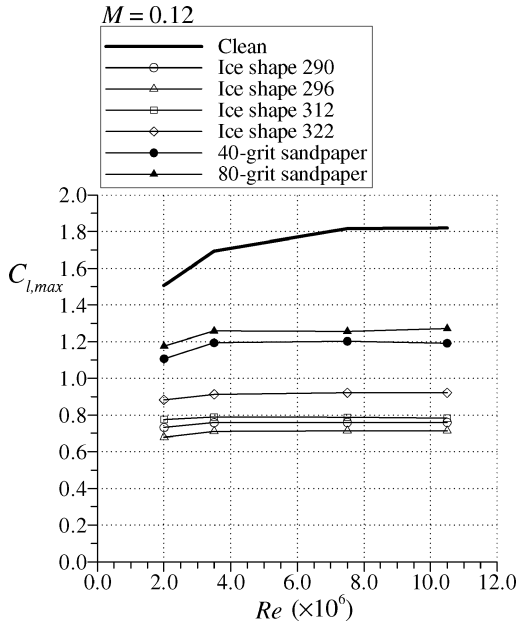

Fig. 13 Effect of Reynolds number on maximum lift for various NACA 23012 airfoil configurations; note that data at $Re = 2.0 \times 10^6$ was at $M = 0.10$.

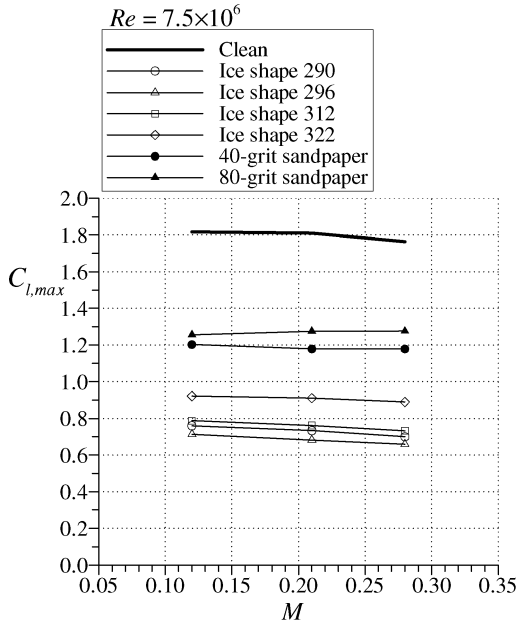

Fig. 14 Effect of Mach number on maximum lift for various NACA 23012 airfoil configurations.

others. For example, Morgan et al.[23] carried out iced-airfoil performance measurements on a multi-element supercritical airfoil. A large glaze-ice simulation made of wood was tested as well as simulated frost that consisted of 70-grit roughness. Performance measurements were carried out with all airfoil elements nested (cruise configuration) at a constant Mach number of 0.20 with $Re = 3.0 \times 10^6$–12×10^6. The results showed very minor changes in maximum lift over the entire Reynolds number range for the iced-airfoil cases. In another study, Addy and Chung[24] tested glaze-ice simulations on an NLF-0414 airfoil in the LTPT. The simulations consisted of castings produced from actual ice accretions (similar to the present study) and corresponding two-dimensional, that is, uniform in the spanwise direction, smoothed shapes produced using rapid-prototyping methods. The ice accretions resulted from a 6- and 22.5-min exposure to the same cloud condition. For three of the four iced-airfoil configurations tested, there was virtually no variation in $C_{l,\max}$ for $Re = 4.6 \times 10^6$–10.5×10^6, at a constant Mach number of 0.21. There was a minor increase in $C_{l,\max}$ over this Reynolds number range for the 22.5-min, two-dimensional ice case. In similar work, Addy et al.[25] tested rime- and glaze-accretion castings resulting from icing sprays of 2.0–22.5 min on a GLC-305 airfoil. Again, there was virtually no dependence of $C_{l,\max}$ on Reynolds number from 3.0×10^6 to 10.5×10^6 at a constant Mach number of 0.21.

The trends observed in the present and previous data further illustrate that the maximum lift of an airfoil with simulated ice, roughness, or other contamination is relatively insensitive to changes in Reynolds number. For an iced airfoil, boundary-layer transition and separation are generally fixed by the size and location of the ice features. This is true once the Reynolds number exceeds a critical value that is dependent on size of the ice accretion or roughness. Lee et al.[26] examined historical roughness data for a NACA 0012 airfoil and suggested that for a typical small-sized ice accretion ($k/c = 0.0009$) this critical Reynolds number was below 0.1×10^6. The data from this and previous studies shows that the Reynolds number variation in iced-airfoil performance is minor relative to the degradation from the clean values.

Mach number effects on iced-airfoil performance has not received as much attention in previous studies. However, Addy and Chung[24] reported lift coefficient results for a Mach number variation from 0.12 to 0.29 at $Re = 6.4 \times 10^6$. There was a slight decrease in $C_{l,\max}$ and α_{stall} with increasing Mach number for all of the ice-shape configurations tested. The magnitude of this decrease is very similar to that shown in the present data. Also consistent were the results of Addy et al.[25] However, the conclusion is identical to that for the Reynolds number effect. The dependence of maximum lift on Mach number in the iced-airfoil case is minor relative to the overall performance degradation caused by the ice accretion.

Ice-Shape Geometry Effects

The large degradation in the maximum lift coefficient for these ice accretions is likely related to the pressure distribution on the NACA 23012 airfoil. Because the clean airfoil has a large suction peak near the leading edge, the airfoil is more sensitive to protuberances in this region. It is likely that an airfoil with a more gradual pressure recovery would have less severe lift degradation due to a similar ice shape. This idea is explained in more detail by Lee,[27] Lee et al.,[26] and Lee and Bragg.[28] For example, a significant feature of ice-shape 296 is the large spanwise ridge located at $x/c \approx 0.04$ (cf. Fig. 3). The effect on the pressure distribution is shown in Fig. 15. The data are for approximately 8-deg angle of attack, which corresponded to α_{stall} for the iced-airfoil case. Figure 15 shows how the

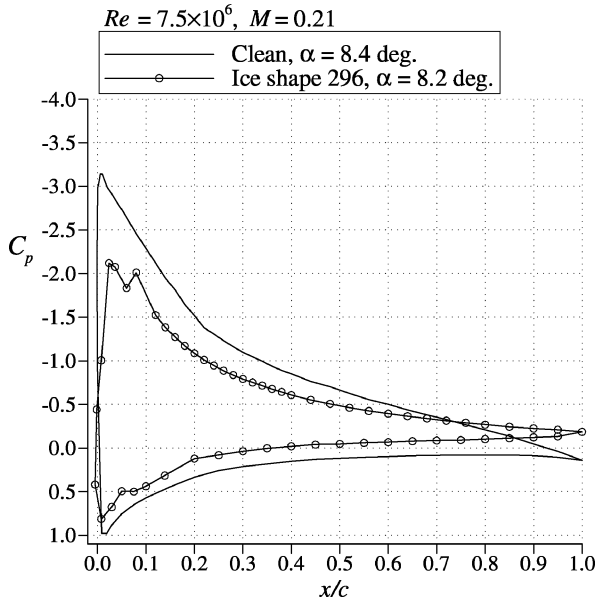

Fig. 15 Comparison of clean and iced NACA 23012 airfoil pressure distributions.

Table 4 Summary of ridgelike features from intercycle ice accretions

Ice shape	Ridge height, k/c	Location, x/c	$C^{a}_{l,\max}$
290	0.0138	0.020	0.734
296	0.0122	0.035	0.682
312	0.0131	0.060	0.761
322	0.0091	0.000	0.911

[a]From the present data at $Re = 7.5 \times 10^6$, $M = 0.21$.

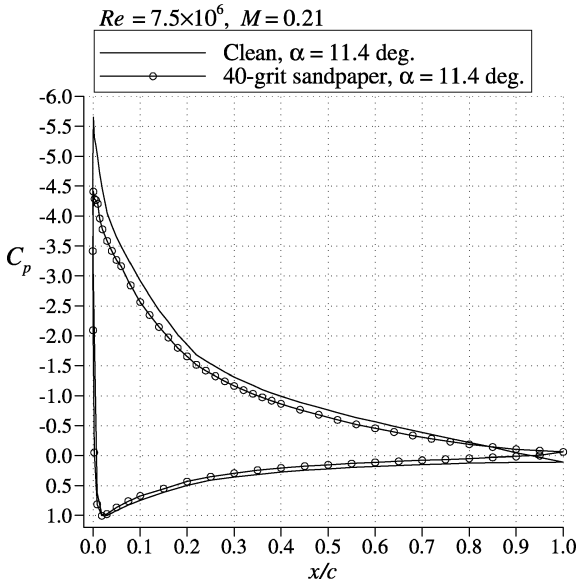

Fig. 16 Comparison of clean NACA 23012 pressure distributions with that having sandpaper over the leading edge.

leading-edge suction pressures were reduced due to the presence of the ice-accretion casting. There was also significant deviation of the lower surface pressure. This behavior is contrasted with the effect of the uniformly distributed roughness shown in Fig. 16. The data are for 11.4-deg angle of attack, which corresponded to α_{stall} for the airfoil with 40-grit sandpaper over the leading edge. The pressure distributions show that there was significant deviations only in the region of minimum pressure. The roughness size of the 40-grit sandpaper tended to be about 10 times smaller than the typical nominal height of the intercycle accretions. In addition, the sandpaper did not simulate the ridgelike protuberance features of the intercycle accretions.

The effect of spanwise-ridge protuberances on airfoil performance has been investigated by others, and some comparison to the present data is warranted. For example, Jacobs[29] parametrically varied the spanwise protuberance height and location on a NACA 0012 airfoil. The data tended to indicate that larger sized protuberances ($k/c > 0.001$) located on the upper surface just aft of the leading edge caused the most significant degradation in maximum lift. Detailed conclusions were not obtainable because of the small number of chordwise protuberance locations tested. Similar results were presented by Lee et al.[26] for tests with a forwardfacing quarter-round on a NACA 23012m airfoil. In this case, where a large number of chordwise locations were tested, the quarter-round protuberance caused the most significant decrease in maximum lift when located at $x/c = 0.10$–0.15.

The dominant ridgelike features of the intercycle ice shapes were obtained using the digitized ice-shape tracings shown in Figs. 2–5. For example, ice-shape 296 (cf. Fig. 3) had a large ridge-like feature located at approximately $x/c = 0.035$ with an approximate height of $k/c = 0.0122$. When the digitized tracing in Fig. 3 was used, the height of this ridge was determined to be $k/c = 0.0122$. Table 4 summarizes the corresponding features extracted from the other ice-shape tracings. The data from Table 4 are plotted along with the aforementioned data of Lee et al.[26] for the NACA 23012m airfoil in Fig. 17. The NACA 23012m is a slightly modified version of the NACA 23012 airfoil used for the present experiments.

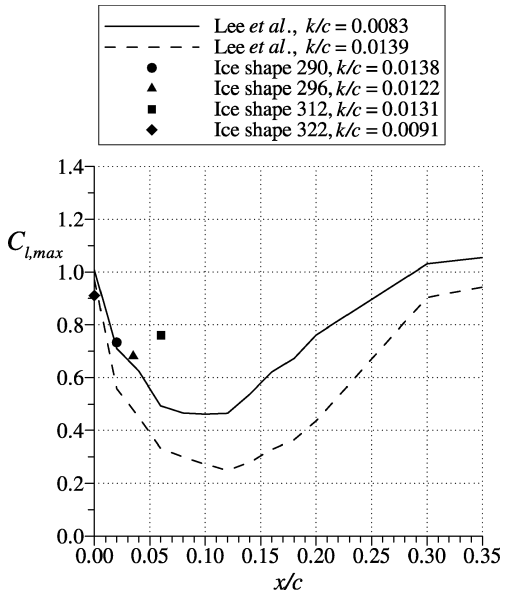

Fig. 17 Comparison of maximum lift data from the present study (at $Re = 7.5 \times 10^6$, $M = 0.21$) with data from Lee et al.[26] at $Re = 1.8 \times 10^6$, $M = 0.18$.

Figure 17 shows that the $C_{l,\max}$ degradation due to the intercycle ice shapes is generally less than for the single quarter-round protuberance. This is true for all of the shapes except 322, which resulted in a lower $C_{l,\max}$ than for the corresponding quarter-round case. This probably occurred because the actual ice shape (cf. Fig. 5) wrapped around the leading edge, covering more surface extent than the Lee et al.[26] quarter-round. For the other three shapes, there are two probable reasons why the loss in $C_{l,\max}$ is not as large for the intercycle ice accretions. The first reason is that the spanwise ridges were not uniform in the case of the intercycle accretions. This is clearly illustrated in Fig. 4 for ice-shape 312, where the ridge is broken in several places along the span. On the other hand, the quarter-round cross section of Lee et al.[26] was invariant across the span. Correspondingly, Fig. 17 shows the most disagreement in $C_{l,\max}$ for this ice shape. Lee[27] investigated the effect of spanwise breaks or gaps for a $k/c = 0.0138$ quarter-round at $x/c = 0.10$. Even relatively small spanwise breaks in the quarter-round caused the $C_{l,\max}$ to increase from 0.27 to approximately 0.50. The second reason is that the quarter-round spanwise ridge caused a large separation region in front of the ridge.[27,28] This was different from the intercycle accretions because the spanwise ridges formed aft of an accretion that covered the entire leading-edge region. This likely reduced the effects of any separated flow region that may have existed immediately upstream of the ridgelike feature. The combined results of this comparison and the uniform roughness testing indicate that any aerodynamic simulation of the intercycle ice accretions should incorporate both the appropriate ice-roughness height and ridgelike features.

Conclusions

The objectives of this study were to characterize the nature of residual and intercycle ice accretions, measure the resulting aerodynamic performance penalties of selected intercycle ice accretions, and, if the penalties were large, determine if more detailed study was warranted. Ice-accretion testing was carried out using a 36-in. chord NACA 23012 airfoil model equipped with a pneumatic deicer. The ice-accretion tests were performed at several different FAR 25 Appendix C cloud conditions. The nominal Reynolds and Mach numbers were 6.5×10^6 and 0.27, respectively. Residual and intercycle ice accretions were generated for 0- and 4-deg angle of attack. These accretions were documented after several deicer cycles to ensure that steady state had been achieved. In select cases, molds were made of the accretions that were later converted into castings for aerodynamic testing. The aerodynamic performance testing was carried out using a similar 36-in. chord NACA 23012

airfoil model over a large range of Reynolds and Mach numbers. A total of four different intercycle ice castings were tested along with the clean configuration. In addition, tests were also conducted with uniformly distributed roughness in the form of 40- and 80-grit sandpaper applied to the airfoil leading edge.

The results of the ice-accretion testing showed that the pneumatic deicer generally cleaned the leading edge well, leaving little residual ice. Therefore, the intercycle accretions tended to have more ice on the leading edge and, in some cases, protuberances on the upper surface. The intercycle ice accretions selected for aerodynamic testing tended to be worst-case scenarios having more ice located on the upper surface. This generally occurred for ice accreted at 0-deg angle of attack and for continuous maximum cases having 3-min deicer cycles.

The simulated intercycle ice accretions caused significant airfoil aerodynamic performance degradation. Maximum lift coefficient values were typically reduced about 60% from 1.8 (clean) to 0.7 (iced), and stall angle values were reduced from 17 deg (clean) to 9 deg (iced). The minimum drag coefficient increased from 0.007 (clean) to 0.026 (iced). An increase in Reynolds number from 2.0×10^6 to 3.5×10^6 caused a small increase in the lift-curve slope and maximum lift coefficient, whereas an increase in Reynolds number from 3.5×10^6 to 10.5×10^6 at a constant Mach number of 0.12 had virtually no effect on any of the performance coefficients. An increase in Mach number from 0.12 to 0.28 at a constant Reynolds numbers of 7.5×10^6 and 10.5×10^6 caused the maximum lift coefficient to decrease only slightly.

The performance degradation due to the 40- and 80-grit sandpaper applied to the airfoil leading edge was substantially less than for the ice-shape simulations. Maximum lift values were reduced about 33% from 1.8 (clean) to 1.2 (with sandpaper) and stall angles were reduced from 17 deg (clean) to 12 deg (with sandpaper). The minimum drag coefficient increased from 0.007 (clean) to 0.011 (with sandpaper). The sandpaper was not large enough to simulate the nominal heights of the intercycle shapes accurately because its roughness was an order of magnitude smaller. Also the sandpaper did not have the ridgelike features of some of the intercycle ice accretions.

The very large performance degradations associated with the intercycle ice shapes implies that more detailed study is warranted. For example, the performance of the NACA 23012 airfoil used here is known to be very sensitive to ice or other contamination in the leading-edge region. The effect of intercycle ice on the performance of other airfoils is largely unknown. Also, the 36-in. chord airfoils used in this study were not representative of a typical wing chord. Therefore, reasonable questions may arise about how the present data would apply to characteristics and resulting performance degradation of ice accretions on a larger scale. This has more to do with the ice accretion geometry because this paper has shown that Reynolds and Mach number effects on performance are very small in the iced case. Because ice accretions and pneumatic boot operation cannot be scaled reliably, full-scale intercycle ice accretions need to be acquired and tested to determine the aerodynamic performance degradation accurately.

Acknowledgments

The authors at the University of Illinois were supported, in part, under Federal Aviation Administration (FAA) Grant DTFA MB 96-6-023, with Jim Riley as the technical monitor. The success of this large collaborative study is due, in part, to the principle participants from the various organizations. The authors wish to thank James Riley and Eugene Hill of the FAA, Thomas Bond of NASA John H. Glenn Research Center and David Sweet and Galdemir Botura of B. F. Goodrich for their key contributions to this research effort. In addition, Timothy Hawk and Tammy Langhals of NASA John H. Glenn Research Center, Peter Brown and the staff of the B. F. Goodrich Icing Wind Tunnel deserve recognition for their efforts during the icing tests and posttest data reduction. The ice-shape castings and pressure instrumentation pieces for the aerodynamic testing were skillfully produced by Phillip Beck and Roger Meredith of NASA John H. Glenn Research Center. The authors also wish to acknowledge the work of test engineers Pamela Phillips and William Sewall and the experienced technicians of the NASA Langley Research Center Low Turbulence Pressure Tunnel.

References

[1]Shin, J., and Bond, T. H., "Surface Roughness Due to Residual Ice in the Use of Low Power Deicing Systems," NASA TM-105971; also AIAA Paper 93-0031, Jan. 1993.

[2]Albright, A. E., Kohlman, D. L., Schweikhard, W. G., and Evanich, P., "Evaluation of a Pneumatic Boot Deicing System on a General Aviation Wing Model," NASA TM-82363, June 1981.

[3]Bowden, D. T., "Effect of Pneumatic De-Icers and Ice Formations on Aerodynamic Characteristics of an Airfoil," NACA TN-3564, Feb. 1956.

[4]Reichhold, J. D., and Bragg, M. B., "Residual Ice Characteristics and the Resulting Aerodynamic Performance Penalties," NASA Advanced General Aviation Transport Experiments (AGATE) WP4.010, Univ. of Illinois, Urbana–Champaign, IL, May 1998.

[5]Gile-Laflin, B. E., and Papadakis, M., "Experimental Investigation of Simulated Ice Accretions on a Natural Laminar Flow Airfoil," AIAA Paper 2001-0088, Jan. 2001.

[6]Jackson, D. G., and Bragg, M. B., "Aerodynamic Performance of an NLF Airfoil with Simulated Ice," AIAA Paper 99-0373, Jan. 1999.

[7]Hill, E. G., "Airplane Deicing Ice Protection Systems, Deicing Boot Ice Bridging, and Airplane Operating Procedures During In-Flight Icing Conditions," Federal Aviation Administration Transportation Airplane Directorate, Feb. 1999.

[8]Hill, E. G., and Reehorst, A. L. (eds.), *FAA/NASA Deicing Boot Ice Bridging Workshop Proceedings*, Ohio Aerospace Inst., Cleveland, OH, 1997.

[9]Riley, J. T., Rios, M. A., Anderson, D., and Dumont, C. J., "A Study of Inter-cycle, Residual and Pre-activation Ice," AIAA Paper 2001-0089, Jan. 2001.

[10]Reehorst, A. L., and Richter, G. P., "New Methods and Materials for Molding and Casting Ice Formations," NASA TM 100126, Sept. 1987.

[11]Broeren, A. P., and Bragg, M. B., "Effect of Residual and Intercycle Ice Accretions on Airfoil Performance," Dept. of Transportation, Federal Aviation Administration Rept. DOT/FAA/AR-02/68, May 2002.

[12]Broeren, A. P., Addy, H. E., Jr., and Bragg, M. B., "Effect of Intercycle Ice Accretions on Airfoil Performance," AIAA Paper 2002-0240, Jan. 2002.

[13]Von Doenhoff, A. E., and Abbott, F. T., Jr., "The Langley Two-Dimensional Low-Turbulence Pressure Tunnel," NACA TN 1283, May 1947.

[14]McGhee, R. J., Beasley, W. D., and Foster, J. M., "Recent Modifications and Calibration of the Langley Low-Turbulence Pressure Tunnel," NASA TP 2328, July 1984.

[15]Paschal, K., Goodman, W., McGhee, R., Walker, B., and Wilcox, P. A., "Evaluation of Tunnel Sidewall Boundary-Layer-Control Systems for High-Lift Airfoil Testing," AIAA Paper 91-3243, Sept. 1991.

[16]Allen, H. J., and Vincenti, W. G., "Wall Interference in a Two-Dimensional-Flow Wind Tunnel, with Consideration of the Effect of Compressibility," NACA Rept. 782, 1944.

[17]Kline, S. J., and McClintock, F. A., "Describing Uncertainties in Single-Sample Experiments," *Mechanical Engineering*, Vol. 75, Jan. 1953, pp. 3–8.

[18]Coleman, H. W., and Steele, W. G., *Experimentation and Uncertainty Analysis for Engineers*, Wiley, New York, 1989, pp. 40–118.

[19]Barlow, J. B., Rae, W. H., Jr., and Pope, A., *Low-Speed Wind Tunnel Testing*, 3rd ed., Wiley, New York, 1999, p. 307.

[20]Ladson, C. L., "Effects of Independent Variation of Mach and Reynolds Numbers on the Low-Speed Aerodynamic Characteristics of the NACA 0012 Airfoil Section," NASA TM-4071, Oct. 1988.

[21]Abbott, I. H., and von Doenhoff, A. E., *Theory of Wing Sections*, Dover, New York, 1959, pp. 124–128, 498, 499.

[22]Drela, M., "XFOIL 6.6 User Primer," Aeronautical and Astronautical Engineering, Massachusetts Inst. of Technology, Cambridge, MA, 14 March 1996.

[23]Morgan, H. L., Jr., Ferris, J. C., and McGhee, R. J., "A Study of High-Lift Airfoils in the Langley Low-Turbulence Pressure Tunnel," NASA TM 89125, July 1987.

[24]Addy, H. E., Jr., and Chung, J. J., "A Wind Tunnel Study of Icing Effects on a Natural Laminar Flow Airfoil," AIAA Paper 2000-0095, Jan. 2000.

[25]Addy, H. E., Jr., Broeren, A. P., Zoeckler, J. G., and Lee, S., "A Wind Tunnel Study of Icing Effects on a Business Jet Airfoil," AIAA Paper 2003-0727, Jan. 2003; also NASA TM-2003-212124, Feb. 2003.

[26]Lee, S., Kim, H. S., and Bragg, M. B., "Investigation of Factors that Influence Iced-Airfoil Aerodynamics," AIAA Paper 2000-0099, Jan. 2000.

[27]Lee, S., "Effect of Supercooled Large Droplet Icing on Airfoil Aerodynamics," Ph.D. Dissertation, Dept. of Aeronautical and Astronautical Engineering, Univ. of Illinois, Urbana, IL, May 2001.

[28]Lee, S., and Bragg, M. B., "Effects of Simulated-Spanwise Ice Shapes on Airfoils: Experimental Investigation," AIAA Paper 99-0092, Jan. 1999.

[29]Jacobs, E. N., "Airfoil Section Characteristics as Affected by Protuberances," NACA Rept. 446, 1932.